Melt Spinning of Metallocene Catalyzed Polypropylenes. I. On-Line Measurements and Their Interpretation

ERIC BRYAN BOND, JOSEPH E. SPRUIELL

Center for Materials Processing and Department of Materials Science and Engineering, The University of Tennessee, 434 Dougherty Engineering Building, Knoxville, Tennessee 37996-2200

Received 23 December 2000; accepted 1 February 2001

ABSTRACT: The melt spinning of metallocene catalyzed isotactic polypropylene resins was investigated. The details are presented for on-line studies performed on six miPP resins with melt flow rates (MFRs) between 10 and 100 and a Ziegler–Natta catalyzed isotactic polypropylene resin with a MFR of 35 for comparison. The on-line studies indicated that, as the molecular weight and polydispersity increased, crystallization occurred closer to the spinneret at higher crystallization temperatures and under lower spin line stresses. Further, as the spinning speed increased, crystallization occurred closer to the spinneret at higher crystallization temperatures because of increased stress in the spin line. These observations were interpreted in terms of an increased rate of crystallization caused by increased molecular orientation in the spin line with increasing molecular weight and increasing spinning speed. This "stress-enhanced" crystallization was further interpreted in terms of an increased rate of crystal nucleation. It was further concluded that the narrower molecular weight distribution of metallocene resins was the primary factor that produced differences in the structure and properties of fibers spun from these resins compared to those of Ziegler–Natta catalyzed resins of similar weight-average molecular weight or MFR. © 2001 John Wiley & Sons, Inc. J Appl Polym Sci 82: 3223–3236, 2001

Key words: metallocene; polypropylene; melt spinning; fiber

INTRODUCTION

The melt spinning of isotactic polypropylene (iPP) into fibers has been studied since the early 1960s and continues today. Much of the early work was reviewed in previous articles from our laboratory and in various review articles.[1–6] The bulk of the earlier published research dealt with resins that were produced by Ziegler–Natta catalyst systems. These polymers were typically high molecular weight, broad molecular weight distribution (MWD) resins as produced in the polymerization reactor. In recent years these resins were frequently given a postreactor treatment to narrow their MWD and lower their molecular weight when they were to be used for fiber spinning. This treatment typically consisted of extrusion in the presence of a peroxide, which produced the desired result by thermal–oxidative degradation of the reactor resin. This process was often referred to as "visbreaking or viscracking." The method is also known as the "controlled rheology process."[7]

A major advantage for the use of metallocene catalysts for preparing PP is that narrow MWD resins can be obtained directly from the reactor without the need for secondary processing. However, the molecular stereoregularity of metallocene catalyzed PPs also differs from that of Ziegler–Natta catalyzed resins. The metallocene

Correspondence to: J. E. Spruiell.
Contract grant sponsor: ExxonMobil Chemical Company.

Journal of Applied Polymer Science, Vol. 82, 3223–3236 (2001)

Table I Resin Molecular Weight Characteristics

Sample Code	Catalyst	MFR	Polydispersity	M_z (kg/mol)	M_w (kg/mol)	M_n (kg/mol)
M10	Metallocene	10	2.65	454.7	256.4	96.8
M22	Metallocene	22	2.25	324.9	192.1	85.4
M32	Metallocene	32	2.28	287.4	172.5	75.6
ZN35	Ziegler–Natta	35	3.29	427.9	189.1	57.5
M45	Metallocene	45	2.83	291.3	164.5	58.2
M70	Metallocene	70	2.53	250.0	141.6	55.9
M100	Metallocene	100	2.27	219.0	123.6	54.5

The melt flow rate (MFR) is in grams/10 minutes at 230°C.

catalyzed resins typically contain regio, as well as stereo, defects and the distribution of defects is fairly uniform from molecule to molecule because of the single-site nature of the metallocene catalysts. This is not the case for Ziegler–Natta catalyzed PPs. For Ziegler–Natta resins the shorter molecules tend to have more defects than the longer, higher molecular weight ones.[8,9] The Ziegler–Natta resins typically contain significant amounts of xylene solubles (atactic molecules), while the metallocene resins have very little atactic content. These differences lead to differences in the quiescent crystallization behavior (kinetics and crystallinity) of the two types of resins.[10] These differences also lead to a significantly lower melting point for the metallocene resins, as measured by a differential scanning calorimeter.[10,11]

The present research was carried out to assess the spinnability of metallocene catalyzed iPP (miPP) resins and to compare the structure and properties of melt-spun fibers produced from them to those produced from Ziegler–Natta iPP (zniPP) resins. In the present study the process variables (except for the take-up velocity) were held constant to elucidate the differences due to resin variables such as the molecular weight and MWD. The results of on-line measurements that were performed to provide insight into the way the structure develops along the spin line are presented and discussed here in Part I, and the final structure and properties of as-spun filaments are described and discussed in the subsequent Part II. The on-line studies included measurements of the diameter and molecular orientation (i.e. birefringence) profiles, the crystallization onset distance from the spinneret, and the stress at crystallization onset. Understanding these important parameters helps in interpreting and understanding the effects of molecular weight moments and process conditions on the development of the structure and properties during melt spinning.

EXPERIMENTAL

Resin Characteristics

Three commercial iPP resins typically used in fiber spinning and four experimental resins were used in the study (ExxonMobil Chemical Company). Six of the resins were prepared with a metallocene catalyst system and the other by a Ziegler–Natta catalyst system. The zniPP resin was "visbroken" with peroxide to lower its average molecular weight and to narrow its MWD. The miPP resins were produced *in situ* with no secondary process step. The molecular weights determined by gel permeation chromatography are given in Table I. The resins were given the sample codes M10, M22, M32, ZN35, M45, M70, and M100; the M stands for metallocene, ZN stands for Ziegler–Natta, and the numbers refer to the melt flow rate (MFR). The miPP polydispersity values ranged from 2.27 for M100 to 2.83 for M45, all of which were narrower than the ZN35 resin. Even though the miPP resins all had very narrow MWDs, their relative differences did become differentiable during fiber spinning, as shown in the following text.

The stereoregularity of these resins was characterized using xylene solubles and carbon-13 NMR. The results are given in Table II. The percentage of xylene solubles was determined according to ASTM D5492-94. The carbon-13 data were obtained at 100 MHz and 125°C on a Varian VXR 400 NMR spectrometer. A 90° pulse, an acquisition time of 3.0 s, and a pulse delay time of 20 s

Table II Stereoregularity Characteristics of Resins

Sample Code	Xylene Solubles (%)	[Meso]	Meso Run Length[a]	Defects/10,000 Units		
				Regio	Stereo	Total
M10	0.60	0.9781	60	91	76	167
M22	0.36	0.9776	68	43	103	146
M32	0.35	0.9752	64	44	113	157
ZN35	3.62	0.9774	102	0	80	80
M45	0.41	0.9756	67	42	107	149
M70	0.48	0.9766	63	38	121	159
M100	1.33	0.9738	52	88	104	192

[a] The number of monomers.

were used. The typical number of transients collected was 2500. The samples were dissolved in tetrachloroethane-d_2 at concentrations between 10 and 15% by weight. Spectral frequencies were recorded with respect to 21.81 ppm for *mmmm*, which was determined with respect to the internal reference tetramethylsilane and close to the reported literature value of 21.855 ppm.

The stereoregularity and xylene solubles data of these resins were discussed elsewhere[10,11]; the data are presented here to illustrate the fundamental differences in the polymer chain molecular architectures of miPP and zniPP resins. Note that ZN35 contains significantly more xylene solubles material than the miPP resins. The defect contents listed in Table II are for the remainder of the resin after removal of the xylene solubles fraction. A comparison of the xylene insoluble fractions showed that the miPP resins contained both regio and stereo defects, and the total number of defects was approximately twice as great as in the zniPP resin.

The thermal properties of these resins are shown in Table III. DSC scans were carried out using a Perkin–Elmer DSC-7 calibrated with an indium standard. The thermal cycle was heating and cooling at 20°C/min, temperature cycling from 0 to 230°C, and a hold time of 5 min at 230°C. The measured melting temperatures of the metallocene catalyzed resins were approximately 13–16°C lower than the ZN35 resin. The quiescent crystallization temperatures for the miPP resins were about 2–3°C lower than for the ZN35 resin.

Preparation of Melt-Spun Filaments

The filaments were spun with the same equipment used in our earlier studies,[1–5] and the reader is referred to these articles for more detail. Generally, monofilaments were spun using an extruder equipped with a constant displacement melt pump that provided a constant extrusion rate. Molten polymer at 210°C as supplied by the

Table III Resin Thermal Property Characteristics

Sample Code	Melting Temperature (°C)		Crystallization Temperature (°C)		Melting Enthalpy (J/g)
	Peak	Onset	Peak	Onset	
M10	149.0	140.8	104.1	109.1	80
M22	150.9	143.4	100.2	105.5	84
M32	150.6	143.2	100.2	105.7	84
ZN35	163.8	152.4	102.6	109.1	91
M45	151.7	144.0	105.4	110.8	87
M70	151.1	143.9	102.4	107.6	88
M100	147.1	140.1	103.6	108.4	81

melt pump was forced through a filter mesh and then through a capillary die with a 0.762-mm diameter and a length to diameter ratio of 5.0. The filament exiting the die was drawn down using an air-jet draw down device similar to Lurgi Docant attenuation devices. The air pressure applied to this device produced high-speed air that provided a drag force to draw the filament down. The amount of drag, and hence the take-up velocity of the filament, could be controlled by varying the air pressure supplied to the draw down device. Depending on the viscous properties of the polymer, spinning speeds of up to about 6000 m/min could be obtained with air pressures up to about 80 psig (551.5 Pa). The distance from the spinneret to the spin line draw down device was kept constant at 2.5 m (250 cm) for all experiments.

The take-up velocities were determined using the continuity equation. Assuming a steady-state spinning process,

$$W = \rho A V = \rho \pi \left(\frac{D^2}{4}\right) V \qquad (1)$$

Here W is the measured mass throughput and ρ is the fiber density. The spinning speed (V) was determined by measuring the on-line filament diameter (D) and the as-spun fiber density. The spinning speed was calculated from the on-line fiber diameter at 2.20 m from the spinneret face. (For the present set of resins, it was observed that the on-line fiber diameter differed from the off-line relaxed diameter by as much as 25%, and the relaxed diameter was greater.) It is important to note that the spinning speed was not the same for each resin at a given draw down pressure. The spinning speed for a particular resin at a given mass throughput and applied air pressure depended on the rheology and crystallization kinetics of the resin.

For the present study the extrusion temperature and mass throughput were kept as constant and consistent as possible for all of the fibers produced. The extrusion temperature was maintained at 210°C and the mass throughput was 1.55 ± 0.03 g/min.

On-Line Measurements

The techniques used to measure the profiles of the diameter and birefringence as a function of distance from the spinneret were previously described[2–5] in detail. The birefringence profiles were measured by mounting a polarizing microscope so that the running filament could pass through the microscope field of view. The microscope was mounted on a movable stand so that it cold be located at various distances from the spinneret. A Berek compensator was then used to measure the retardation of the filament at each position. The diameter profiles were measured with a Zimmer diameter monitor that also moved along the running spin line. The instrument operated on a noncontact electrooptic principle and had a diameter resolution of ±0.5 μm.

Small Angle X-Ray Scattering (SAXS) Measurements

The SAXS measurements were carried out at Oak Ridge National Laboratory's 10-m SAXS instrument[12] using a source to sample distance of 3 m and a sample to detector distance of 5 m. The X-ray generator was operated at 100 mA and 40 kV using CuKα radiation (0.1542 nm). The data were Lorentz corrected prior to computing the long periods. Other details of the experimental measurements are given elsewhere.[11]

RESULTS AND DISCUSSION

On-Line Birefringence Measurements

The filament birefringence as a function of distance from the spinneret is shown for the various resins in Figures 1–3 at air pressure settings of 5, 15, and 25 psig (34.5, 103.4, and 172.4 Pa), respectively. The birefringence was a direct measure of the total molecular orientation present in the filaments. These data showed that the orientation developed closer to the spinneret as the molecular weight of the metallocene resin increased at all three draw down pressures. The behavior of ZN35 was interesting. At the low draw down pressure shown in Figure 1, its birefringence developed slightly closer to the spinneret than did M32 and somewhat farther from the spinneret than M22. With an increase in the draw down pressure to 15 psig, the development of the birefringence shifted closer to the spinneret for all resins, compared to 5 psig. However, the shift in the ZN35 resin was much greater than that of the metallocene resins and, under these spinning conditions, it developed its birefringence closer to the spinneret than any of the metallocene resins, including M10. At a draw down pressure of 25 psig the distance from the spinneret at which the birefringence developed for the ZN35 resin changed little compared to the 15 psig data, but the bire-

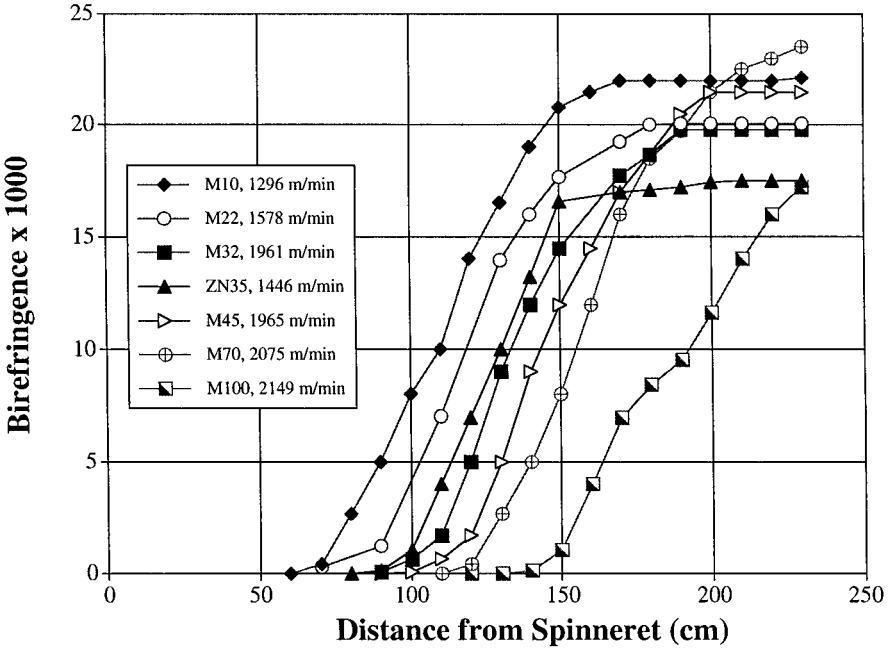

Figure 1 The on-line birefringence versus the distance from the spinneret for a draw down pressure of 5 psig (34.5 Pa).

fringence profiles for the metallocene resins had all moved closer to the spinneret. In this case M10 developed its birefringence at about the same distance from the spinneret as the ZN35 resin. The ZN35 resin behavior can be traced to its broader MWD compared to the metallocene resins. It was shown earlier for Ziegler–Natta PPs that the birefringence developed closer to the spinneret as the polydispersity increased.[3] The reasons for this are further discussed below.

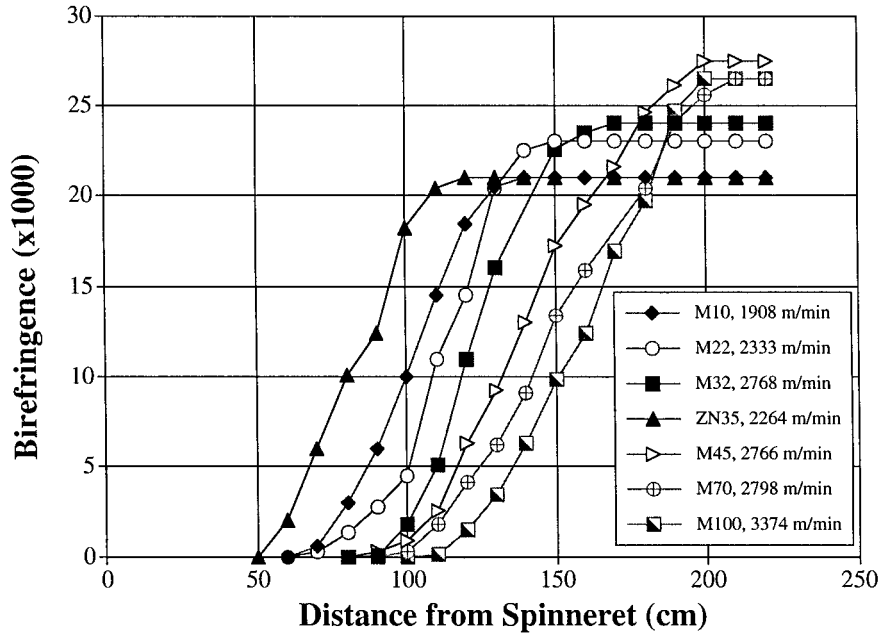

Figure 2 The on-line birefringence versus the distance from the spinneret for a draw down pressure of 15 psig (103.4 Pa).

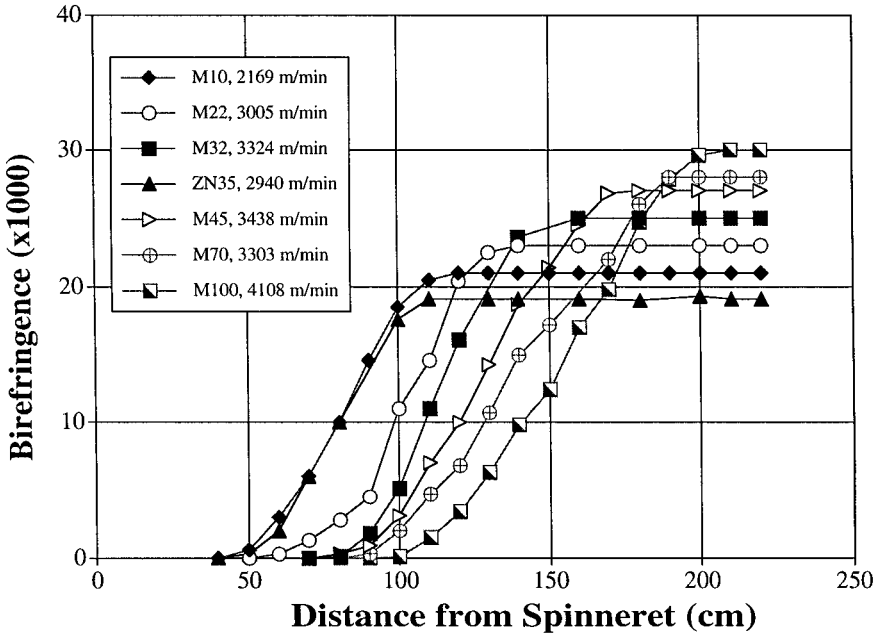

Figure 3 The on-line birefringence versus the distance from the spinneret for a draw down pressure of 25 psig (172.4 Pa).

At some distance from the spinneret that differed for each resin, the birefringence had a plateau value that was close to that measured off-line on the as-spun filaments. It is worth noting that this final birefringence increased with the decrease of the weight-average molecular weight (increase of the MFR) of the metallocene resins at a given draw down pressure. A partial explanation for this is that the spinning speed (take-up velocity) increased at a given draw down pressure as the molecular weight decreased for the metallocene resins. (Note that the take-up velocity of each resin is indicated in the legends of Figs. 1–3.) This was due to the decrease of the resin viscosity as the weight-average molecular weight decreased. Also, because the structure was developing further from the spinneret with a decrease of the molecular weight, it was developing at a lower temperature. The combination of a higher spin-draw (higher take-up velocity) and a lower temperature of the filament during the important structure development stage produced higher final birefringence as the molecular weight decreased (MFR increased). The fact that the structure of the Ziegler–Natta resin developed closer to the spinneret and therefore at higher temperature in the spin line than a metallocene resin of similar weight-average molecular weight and MFR appeared to be largely responsible for the lower final birefringence of the ZN35 resin compared to the metallocene resins.

Further Interpretation of Birefringence Measurements

A considerable amount of information can be learned by studying the orientation development of a running filament using on-line birefringence measurements. Previous studies[2–5,13] showed that the sudden rapid rise in the birefringence versus the distance from the spinneret profile is a strong indication of crystallization occurring in the spin line. The growth of crystals from oriented nuclei during stress-enhanced crystallization causes a rapid increase in orientation and birefringence.[2–5,13,14] As crystallization is completed the rate of increase in orientation and, hence the birefringence, approaches zero. Therefore, on-line birefringence measurements can be used to estimate where crystallization starts and when crystallization is largely completed. In the following we assumed that crystallization onset occurred near the position in the spin line where the birefringence rapidly increased from a small value near zero. Crystallization was essentially complete when the birefringence leveled off to a relatively constant final value.

The on-line birefringence study at 5 psig in Figure 1 shows that crystallization began for M10

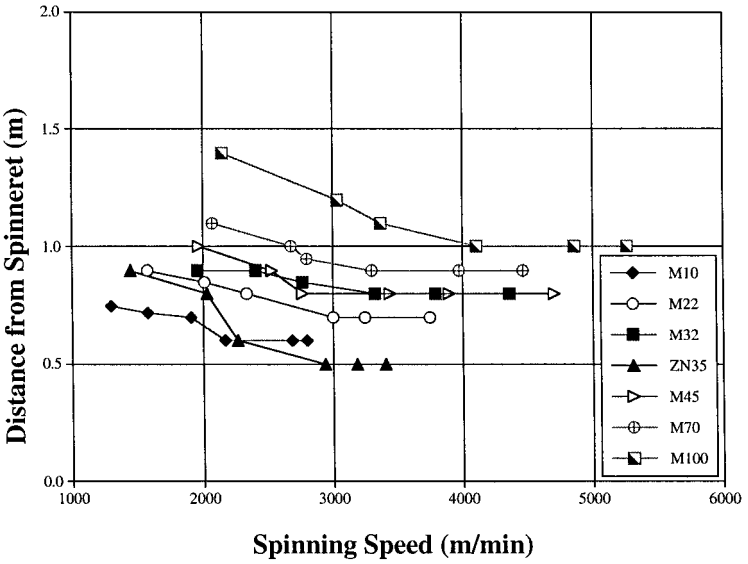

Figure 4 The distance from the spinneret of crystallization onset versus the spinning speed.

at a distance from the spinneret of approximately 70 cm, followed by M22, ZN35, M32, M45, M70, and finally M100 at a distance of 140 cm from the spinneret. The variation in crystallization distances was 70 cm. Figure 2 shows that at a draw down pressure of 15 psig ZN35 began crystallization closest to the spinneret, followed by M10, M22, M45, M32, M70, and M100. Furthermore, the miPP resins crystallized closer to the spinneret with increasing molecular weight. Increasing the draw down pressure to 25 psig, as indicated in Figure 3, induced crystallization closer to the spinneret for all resins. At 25 psig the M10 and ZN35 both began crystallizing at 50 cm, followed by M22, M45, M32, M70, and M100 at 100 cm.

Figure 4 shows the distance from the spinneret at which crystallization began as a function of the spinning speed. The crystallization onset distance moved closer to the spinneret face as the spinning speed increased and generally with increasing molecular weight. At the higher spinning speeds for each resin the distance from the spinneret at which the resin started to crystallize became constant. This suggested that either the crystallization rate was saturated at some stress level or that a further increase in the crystallization rate due to increased stress was offset by the effect of the increased cooling rate of the fibers moving at faster speeds through the ambient air.

The onset distance of crystallization for M45 and ZN35 in Figure 4 shows the effects of their higher polydispersity values. As the spinning speed increased for a broader MWD resin, the larger molecular weight chains became oriented faster because of the larger relative number of entanglements. Relative to another resin with a narrower MWD and the same weight-average molecular weight, a broader MWD resin had a greater population of higher molecular weight chains, commonly referred to as the high molecular weight tail. For a broader MWD resin the high molecular weight chains aligned with one another and with the draw down direction earlier in the spin line than a similar narrow MWD resin. The oriented high molecular weight chains could then initiate the growth of row nuclei closer to the spinneret, which initiated the crystallization process. In contrast, a more uniform MWD produced a more uniform and gradual alignment of the molecules in the melt, and at the same average molecular weight it resulted in a smaller amount of early preferential alignment. Therefore, with a broader MWD the M45 and ZN35 initiated crystallization closer to the spinneret, even though they had lower weight-average molecular weights compared to M32 and M10, respectively.

The effects of the MWD were reported elsewhere with a similar result[3] using similar reasoning. The present results showed that this effect was important in distinguishing the difference in spinning behavior of the miPP resins from zniPP resins of similar MFR and/or weight-average molecular weight. The fact that the higher molecular weight chains in Ziegler–Natta resins contained

fewer defects may also be of some significance in generating early nucleation. But we believe that the difference in MWD was primarily responsible for the difference in spinning behavior between the Ziegler–Natta resins and the metallocene catalyzed resins.

Figure 5 shows a plot of the stress in the spin line at the point of crystallization onset versus the spinning speed for the resins. In order to obtain the rheological stress at the point of crystallization, the filament tension at the take-up device (F_L) was first measured by a tensiometer. The rheological force at the point of crystallization was then computed from the equation

$$F_{\text{rheo}}(z) = F_L - \int_z^L \rho_{\text{air}} C_d V^2 \pi D \, dz - W[V(L) - V(z)] + \int_z^L \rho g \pi \left(\frac{D^2}{4}\right) dz \quad (2)$$

where C_d is the air drag coefficient, ρ_{air} is the density of air, g is the acceleration due to gravity, and the other symbols were previously defined. The stress was obtained by dividing the rheological force at the point of crystallization by the measured filament diameter at that point. The data showed that the stress at crystallization onset increased with the spinning speed. The data for all the resins studied fell within a fairly narrow band of stresses as a function of the spinning speed, indicating that, at a given spinning speed, the stress at crystallization onset was essentially independent of the molecular weight, at least for the resins in this study. Note that the data for the ZN35 resin fell at the bottom of the band for the metallocene resins; this may have been due to its broader MWD.

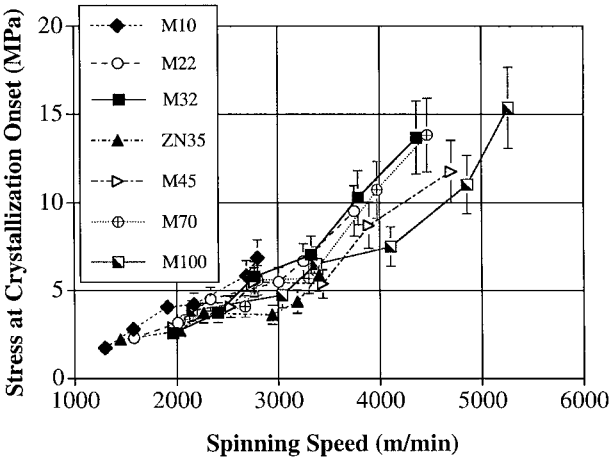

Figure 5 The stress at crystallization onset versus the spinning speed.

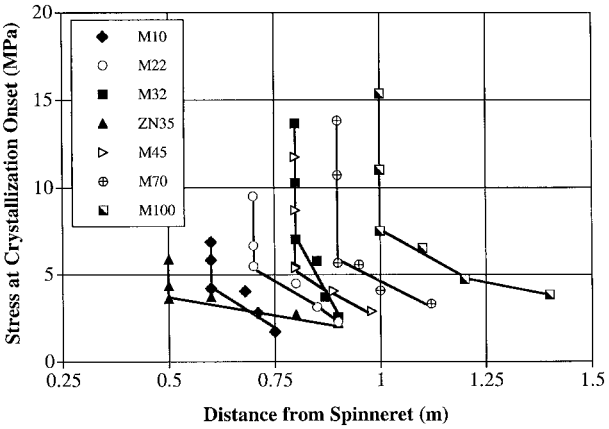

Figure 6 The stress at crystallization onset versus the distance from the spinneret.

Figure 6 shows the stress at crystallization onset as a function of the distance from the spinneret. The data fell in bands according to the resin molecular weight and polydispersity, and the higher molecular weight and broader MWD resins crystallized closer to the spinneret. The order was ZN35, M10, M22, M45, M32, M70, and M100. It is important to note here that the temperature of crystallization decreased with increasing distance from the spinneret, so that crystallization of the lower molecular weight material occurred at lower temperature and higher supercooling. In order to get a given resin to crystallize closer to the spinneret, it is necessary to increase the stress in the spin line or to increase the thermal driving force by more rapid cooling. One method of increasing the stress is to increase the spinning speed as illustrated in Figure 5. However, Figure 6 shows that the stress required rapidly increases as the distance from the spinneret decreases, provided the cooling parameters stay the same. Thus, there is a physical limitation as to how close to the spinneret a given resin can be crystallized under given cooling parameters. This limiting distance is a strong function of the molecular weight.

Note also that the stress needed to attain crystallization tends to increase with a decrease in the molecular weight. This is presumably related to the lowering of the viscosity and relaxation time. Cooling to a lower temperature (and greater

distance from the spinneret) increases both the driving force for crystallization and the viscosity of the resin. This allows the resin to crystallize.

The results of the on-line studies thus far are reasonable when the rheology of the resins is considered. As the molecular weight increases, the relaxation time and chain entanglement density increases. Studies indicated[5,15] that full relaxation does not occur in PP melts during a high speed cooling process, because the crystallization times are too short. Therefore, higher molecular weight chains would be statistically more probable to produce a critical nucleus at any given temperature and process condition. We observed that broader MWD resins initiate nucleation closer to the spinneret because of the formation of row nuclei, as discussed earlier. Research indicated that higher molecular weight chains are more likely to produce a critical nucleus, even under quiescent conditions attributable to athermal nucleation.[15]

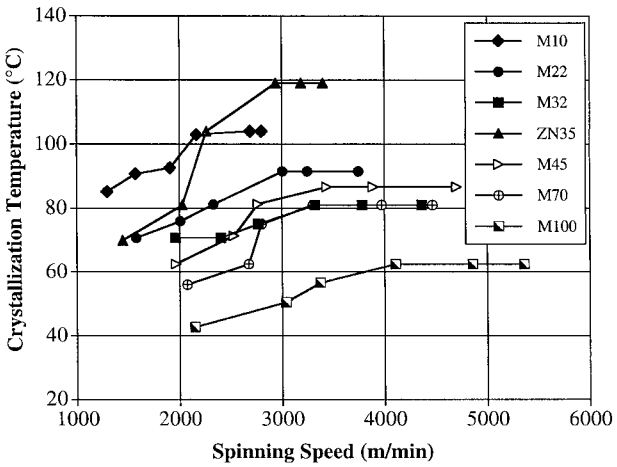

Figure 7 The filament crystallization temperature determined from a combination of a computer simulation of the temperature profile and the experimental distance from the spinneret at which crystallization was observed.

Estimation of Crystallization Temperature from Modeling and Long Period

Because we were unable to determine the crystallization temperature directly, we used two approaches to estimate the crystallization temperature by indirect means. First we used a spin line modeling program developed in our laboratory[16–18] to compute the temperature profile along the spin line in the absence of crystallization. This procedure involved entering the appropriate elongational viscosity function, heat transfer conditions, and spinning parameters into the model and solving the system of simultaneous equations for the temperature profile. For the purpose of this calculation the heat of crystallization was set equal to zero, so that crystallization in the model would not perturb the calculated temperature profile. The data of Figure 4 for the distance from the spinneret at which the crystallization began was used in combination with the calculated temperature profile to estimate the temperature at which crystallization began for each resin and spinning condition. The results of this approach are shown in Figure 7. The results indicated that the crystallization start temperature tended to increase with the take-up velocity. This was a clear indication of the presence of molecular orientation enhanced crystallization, because higher take-up velocities produce faster cooling of the filament, which in the absence of stress and molecular orientation would result in greater supercooling and crystallization at lower temperatures. At a given take-up velocity, the temperature at which crystallization starts increases with the increase of both the molecular weight and the polydispersity. Comparing the result for M10 with that for M100 indicated a difference in crystallization start temperature that was about 40°C between these two resins. This clearly showed the significance of higher molecular weight and higher viscosity in generating conditions for stress-induced crystallization. The effect of polydispersity was related to the influence of the high molecular weight tail in making it possible to form row nuclei at higher temperatures, as described above.[3]

The second approach involved estimating the on-line crystallization temperature by determining the crystal lamella thickness of the as-spun fibers from the long period using SAXS. The long periods of fibers spun from selected resins as a function of spinning speed are given in Table IV. The lamella thickness in Table IV was obtained by multiplying the long period by the percentage of crystallinity as determined by the density. Further, in order to estimate the crystallization temperature from the measured lamella thickness, a plot of the measured lamella thickness versus the measured crystallization temperature was constructed for films crystallized at high cooling rates and quiescent conditions using the technique described by Ding and Spruiell.[19] This technique gives very accurate measurement of the

Table IV Crystalline Fraction, Long Period, and Lamellae Thickness of Selected Melt-Spun Filaments

Sample Code	Spinning Speed (m/min)	Density (g/cm^3)	Crystalline Fraction	Long Period (nm)	Lamella Thickness (nm)
M10	1296	0.9009	0.5717	11.3	6.5
	1572	0.9019	0.5840	11.6	6.8
	1908	0.9032	0.6000	11.9	7.1
	2169	0.9032	0.6010	12.0	7.2
	2690	0.9034	0.6031	12.0	7.2
	2800	0.9033	0.6024	12.0	7.2
M22	1578	0.9013	0.5765	10.7	6.2
	2008	0.9018	0.5828	10.9	6.3
	2333	0.9022	0.5879	11.0	6.5
	3005	0.9030	0.5980	11.5	6.9
	3248	0.9038	0.6081	11.6	7.1
	3748	0.9043	0.6144	11.7	7.2
M32	1961	0.8909	0.4434	10.0	4.4
	2405	0.8918	0.4548	10.7	4.9
	2768	0.8936	0.4781	10.8	5.2
	3324	0.8973	0.5252	11.2	5.9
	3786	0.9001	0.5617	11.5	6.4
	4363	0.9011	0.5740	11.4	6.5
ZN35	1446	0.8935	0.4772	11.4	5.4
	2030	0.8964	0.5138	12.0	6.2
	2264	0.8980	0.5339	12.2	6.5
	2940	0.9004	0.5655	13.3	7.5
	3187	0.9018	0.5828	13.6	7.9
	3401	0.9023	0.5894	12.6	7.4
M100	2149	0.8913	0.4479	9.6	4.3
	3040	0.8922	0.4596	10.4	4.8
	3374	0.8937	0.4789	10.3	5.0
	4108	0.8955	0.5029	10.5	5.3
	4858	0.8976	0.5299	10.7	5.7
	5261	0.8980	0.5350	10.9	5.8

temperature at which the bulk of the crystallization process occurs by virtue of having a thermocouple imbedded directly in the sample. Because of the release of the heat of crystallization, a plateau was observed in the temperature profile during a major portion of the crystallization process. This temperature was taken as the temperature of crystallization for the films. These crystallization data for films can be found elsewhere.[20] It was assumed for the purpose of this analysis that the lamella thickness was determined only by the crystallization temperature, whether under quiescent crystallization conditions or otherwise. A curve fit of the quenched film data allowed the crystallization temperature of the as-spun fibers to be estimated from the measured lamella thickness. The crystallization temperature of M45 and M70 could not be determined using this method because these resins were not studied under quiescent nonisothermal conditions. Although this approach can be criticized, it does provide a reasonably valid and useful method for approximating the crystallization temperature of the fibers. The results of this method are shown in Figure 8.

Comparing the data of Figure 7 to those of Figure 8, we see that the trends are remarkably similar for the two figures. Careful inspection shows that the crystallization temperatures determined from the long periods (Fig. 8) were generally lower than the values determined from the model calculation. A logical explanation for this difference is that the temperatures given in Figure 7 are for the *start* of crystallization, while the values in Figure 8 tend to reflect the average temperature at which the lamellae formed. This

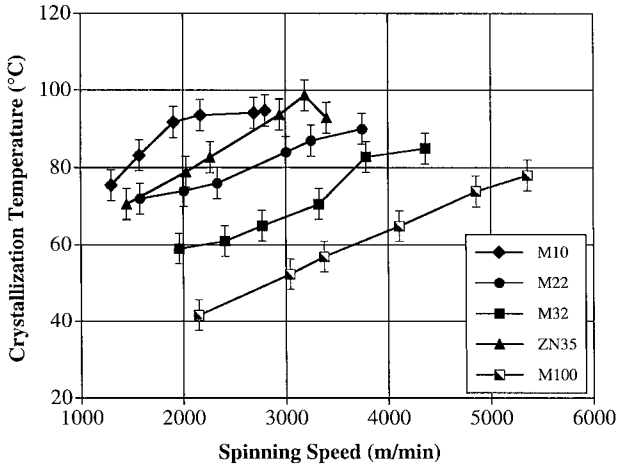

Figure 8 The filament crystallization temperature determined from the lamella thickness.

temperature would be expected to be lower than the crystallization start temperature for crystallization under the very nonisothermal conditions found in the spin line.

It is well known that solidification of PP at temperatures below about 70°C causes a transition from the formation of the α-monoclinic form to the disordered smectic form. Based on the data in Figures 7 and 8, one would expect the smectic form became more prominent in the as-spun fibers as the spinning speed, molecular weight, and polydispersity decreased. Wide angle X-ray patterns to be described in part II confirmed this expectation. Because polydispersity plays an important role in determining the crystallization temperature, it was expected and observed that the narrow molecular weight miPP resins would form the smectic form at higher spinning speeds than a zniPP with similar weight-average molecular weight or MFR. The X-ray patterns also confirmed this expectation. They were also consistent with substantial smectic phase formation in fibers for which the crystallization temperature of Figure 8 is below about 70°C.

Discussion of Stress-Induced Crystallization

Stress-induced (or stress-enhanced) crystallization is the concept that was responsible for the massive acceleration of crystallization kinetics observed in the spin line. Stress-enhanced crystallization results from molecular orientation of the melt in the spin line. Previous research[1–5,13,14,21,22] showed that the effect of stress on the crystallization kinetics increased as the molecular weight and polydispersity increased. Because quiescent nonisothermal crystallization kinetics data were available for several of the present resins, it was insightful to estimate the effects of molecular orientation on the crystallization process in the spin line for the current set of resins.

Crystal nucleation density is the major component of bulk crystallization kinetics that is expected to change significantly with molecular orientation in the spin line. Therefore, we calculated the influence of orientation on the *effective* nucleation density. The ratio of the effective nucleation density of an oriented sample to that of an unoriented sample at the same crystallization temperature was calculated for selected resins using an Avrami type relationship for the overall crystallization kinetics.

The on-line fiber spinning studies were used to calculate the oriented nucleation density that occurred during spinning of the fibers, and the unoriented nucleation density was computed using the quiescent nonisothermal half-time data obtained using the high cooling rate nonisothermal technique of Ding and Spruiell.[19] The details of this high cooling rate nonisothermal study will be described in a future article and can also be found in the literature.[20]

The specific manner in which each nucleation density was determined is explained in the following text.

Fiber Spinning. The on-line birefringence measurements were used to determine the crystallization half-time (Figs. 1–3). The onset of crystallization was determined as previously described. Crystallization was assumed to be complete when the birefringence leveled off. The total crystallization time was calculated by dividing the distance in the spin line between the onset and completion of crystallization by the spinning speed. This was divided by 2 to obtain the half-time. This approach was obviously an oversimplification, but it gave an estimate of the crystallization half-time that should be consistent from resin to resin.

Sporadic nucleation was chosen as the nucleation mechanism with disk-shaped growth geometry. Sporadic nucleation was chosen because the nucleation is assumed to be homogenous (and not a result of nucleating agents, either intentionally added or otherwise), a result of an oriented melt accelerating the nucleation process. Studies also showed that the crystal growth morphology is disk shaped (i.e., cylindrical) at high spinning

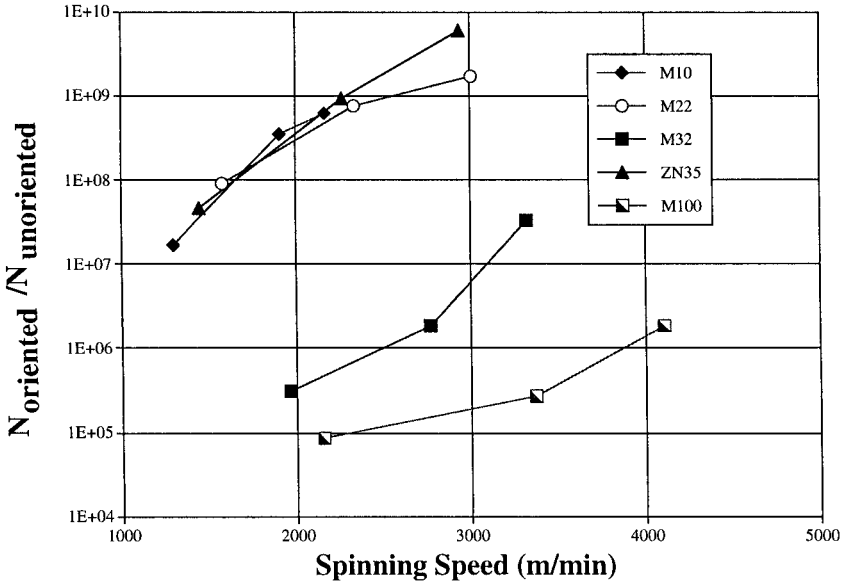

Figure 9 The ratio of the oriented nucleation density to the unoriented nucleation density versus the spinning speed.

speeds.[1–5,13,14] The Avrami rate constant (K) for these assumptions has the form

$$K = \frac{\pi}{3}\dot{N}G^2D \tag{3}$$

where $\dot{N}$ is the nucleation rate constant, G is the linear growth rate, and D is the disk thickness.

Rearranging to obtain the nucleation rate gives

$$\dot{N} = \frac{3K}{G^2D\pi} \tag{4}$$

The disk thickness was taken to be the same as the lamellae thickness for the fiber samples. The growth rate was obtained from a curve fit of the growth rate versus the crystallization temperature determined from the high cooling rate experiments described elsewhere.[20] The crystallization temperature for each fiber sample was determined from Figure 8. The on-line fiber spinning crystallization rate constant was calculated using the crystallization half-time of each fiber sample, assuming an Avrami exponent of 3. The nucleation rate was converted into the nucleation density (N) by multiplying the nucleation rate by the total crystallization time.

The results of the nucleation density in the running spin line were similar if instantaneous nucleation was assumed. The numerical value was not identical, but the order of magnitude was similar and would not appreciably affect the oriented to unoriented nucleation density ratio calculations and conclusions.

Quiescent Nonisothermal. The quiescent nonisothermal nucleation density was calculated to simulate the behavior of the same material under quiescent conditions and at similar crystallization temperatures as occurred for the fibers. The growth mechanism was assumed to be sporadic in nature and to have the growth geometry of a sphere. From the Avrami rate constant for this case we obtain

$$\dot{N} = \frac{3K}{G^3\pi} \tag{5}$$

The same growth rates used in the fiber spinning calculation were used in the present calculation. An Avrami exponent of 4 was used in the calculation of the crystallization rate constant for sporadic spherulitic growth.

The results of the above-described calculations are presented in Figure 9. They clearly show that the higher molecular weight resins had a significantly higher ratio of oriented to unoriented nucleation density than the lower molecular weight resins. At spinning speeds above 2000 m/min even the M100 resin had at least a 10^5 increase in

nucleation, which showed the huge effect of molecular orientation in accelerating the crystallization rate.

As pointed out in this work, ZN35 had a MFR that was approximately equal to M32. When comparing M32 and ZN35 molecular weight characteristics, the weight-average molecular weights differed by only 7%, while the number averages differed by 25%. A comparison of the fiber on-line spinning properties of these two resins clearly illustrates the powerful effects of MWD in affecting the crystallization process. The data of Figure 9 further illustrates the major effect of the broader MWD of ZN35 in nucleating the crystallization in the spin line in comparison to M32.

One factor that affected the fiber formation, which has not been explicitly addressed, was the effect of crystal growth rates. In the above discussion it was assumed that the crystal growth rates were the same for lamellae grown from an oriented melt as for those grown from an unoriented melt. This cannot be entirely accurate, but the change was expected to be small compared to the change in the nucleation rate. Differences of quiescent growth rate among the different resins were included in the calculation by using the growth rates measured during quiescent crystallization for each resin. Although small differences in growth rates were observed among the miPP resins, there was a more significant difference between the observed growth rates of ZN35 compared to the metallocene catalyzed resins and the growth rates for ZN35 were substantially greater than for any of the miPP resins. This was apparently related to the differences in stereoregularity of the high molecular weight chains (see Table II). These differences are discussed in detail elsewhere[20,23] for quiescent crystallization. In general, we expected that differences in the growth rates would be reflected in the half-time for crystallization. However, within the assumptions made above, these differences should have had little effect on the nucleation density ratios of Figure 9.

In terms of the rate of development of the structure in melt-spun filaments, we would anticipate that slower crystal growth rates would tend to decrease the slope of the birefringence curves in the rapidly rising portion of the profiles plotted in Figures 1–3. This effect was observed when the growth rates were reduced by random copolymerization of PP with a few percent of ethylene.[4,5] Aside from a gradual decrease that could be attributed to the effect of a lower crystallization temperature, we did not observe major differences in the slopes of Figures 1–3 in the region after crystallization had begun. Thus, we do not believe that differences in the lamellae growth rates were a significant factor in the present results on homopolymer samples. This further suggests that the differences in defect type and distribution were of much less importance in controlling the structure and properties of melt-spun fibers for the present metallocene resins than were the changes in resin rheology. However, this is not to say they are never important in fiber spinning. At very low spinning speeds, where the stress levels are very low in the spin line and nucleation rates are much closer to those found in quiescent samples, the effects of differences in lamellae growth rates are likely to be more important.

Thus, we may conclude that changes in the nucleation density (i.e., the formation of row nuclei) caused by the influence of molecular orientation explains the observed differences between the resins. The differences in molecular orientation resulted from differences in the molecular weight and MWD. Thus, the difference in fiber spinning behavior between metallocene resins and Ziegler–Natta resins of similar molecular weight appeared to be largely associated with the difference in MWD.

CONCLUSIONS

A study of fiber formation in a series of metallocene catalyzed iPPs was carried out using on-line measurement of the diameter and birefringence profiles as the primary tools of investigation. The results of this study showed that the molecular weight and MWD of iPP resins had a significant influence on the development of the structure and properties of fibers prepared from these resins. The narrower MWD of metallocene resins appeared to be the primary factor that produced differences in the structure and properties of fibers spun from these resins compared to those of Ziegler–Natta catalyzed resins of similar weight-average molecular weight or MFR.

Specifically, the on-line studies using diameter and birefringence measurements showed that orientation development and crystallization occurred closer to the spinneret as the draw down pressure, spinning speed, molecular weight, or polydispersity increased. The crystallization temperature also tended to increase as the spinning

speed, molecular weight, and polydispersity increased. This behavior was attributed to the phenomenon of stress-enhanced crystallization. The stress required to get crystallization to occur at a given distance from the spinneret appeared to decrease as the molecular weight of the resin increased. This behavior appeared to be related to the higher chain entanglement density and greater relaxation time for the higher molecular weight resins. This allowed crystal nuclei to occur at higher temperature for the higher molecular weight resins. In a similar way the high molecular weight tail in resins with broader MWDs also allowed fibril nuclei to form at higher temperature than for a narrower distribution resin of equivalent weight-average molecular weight or MFR.

Estimates of the bulk nucleation densities showed that the nucleation density for oriented samples was generally many orders of magnitude higher than for quiescent samples crystallized at the same temperature. The ratio of the nucleation density of oriented fibers to that of samples crystallized under quiescent conditions increased with the take-up velocity or molecular weight.

A further description of the final structure and properties of these fibers will be presented in part II of this series.

The authors wish to thank ExxonMobil Chemical Company for supplying the resins and for financial support of this research. We are indebted to Dr. J. C. Randall (ExxonMobil) for performing the stereoregularity measurements. We especially thank J. C. Randall, Allan Stahl, C. Y. Cheng, and G. C. Richeson for numerous discussions of significant issues related to this research.

REFERENCES

1. Lu, F.-M.; Spruiell, J. E. J Appl Polym Sci 1987, 34, 1521.
2. Lu, F.-M.; Spruiell, J. E. J Appl Polym Sci 1987, 34, 1541.
3. Misra, S.; Lu, F.-M.; Spruiell, J. E.; Richeson, G. C. J Appl Polym Sci 1995, 56, 1761.
4. Spruiell, J. E.; Lu, F.-M.; Ding, Z.; Richeson, G. C. J Appl Polym Sci 1996, 62, 1965.
5. Lu, F.-M.; Spruiell, J. E. J Appl Polym Sci 1993, 49, 623.
6. White, J. L.; Cakmak, M. Adv Polym Technol 1986, 6, 295.
7. Steinkamp, R. A.; Grail, T. J. (to Exxon Research and Engineering). U.S. Pat. 3,862,265, 1975.
8. Moore, E. P., Jr. In Polypropylene Handbook; Hanser: New York, 1996; p 403.
9. Richeson, G. C.; Stahl, G. A.; Plank, D. A.; Cheng, C. Y. Nonwovens World 1998, Summer, 76.
10. Bond, E. B.; Spruiell, J. E. ANTEC Proceedings; Society of Plastics Engineers: Brookfield, CT, 1997, XLIII, 1754.
11. Bond, E. B.; Spruiell, J. E. J Polym Sci Part B: Polym Phys 1999, 37, 3050.
12. Wignall, G.; Lin, J. S.; Spooner, S. J Appl Crystallogr 1990, 23, 241.
13. Nadella, H. P.; Henson, H. M.; Spruiell, J. E.; White, J. L. J Appl Polym Sci 1977, 21, 3003.
14. Dees, J. R.; Spruiell, J. E. J Appl Polym Sci 1974, 18, 1053.
15. Ziabicki, A. Colloid Polym Sci 1996, 274, 705.
16. Patel, R. M.; Jayendra Bheda, J.; Spruiell, J. E. J Appl Polym Sci 1991, 42, 1671.
17. Hajji, N.; Spruiell, J. E.; Lu, F. M.; Malkan, S.; Richeson, G. C. INDA J Nonwovens Res 1991, 4, 16.
18. Ding, Z. Ph. D. Dissertation, University of Tennessee, 1996.
19. Ding, Z.; Spruiell, J. E. J Polym Sci Part B: Polym Phys 1996, 34, 2783.
20. Bond, E. B. Ph.D. Dissertation, University of Tennessee, 1999.
21. Fan, Q.; Xu, D.; Zhao, D.; Qian, R. J Polym Eng 1985, 5, 95.
22. Shimizu, J.; Okui, N.; Kikutani, T. In High Speed Fiber Spinning; Ziabicki, A., Kawai, H., Eds.; Wiley-Interscience; New York, 1985; p 429.
23. Bond, E. B.; Spruiell, J. E. unpublished manuscript.